Energy & Environmental Science

Accepted Manuscript

This article can be cited before page numbers have been issued, to do this please use: Z. Lv, R. Tang, C. Sun, W. meng, J. Yang, S. Li, Q. Wu, M. Zhang, J. Zhao and Y. Yang, *Energy Environ. Sci.*, 2024, DOI: 10.1039/D4EE03857F.

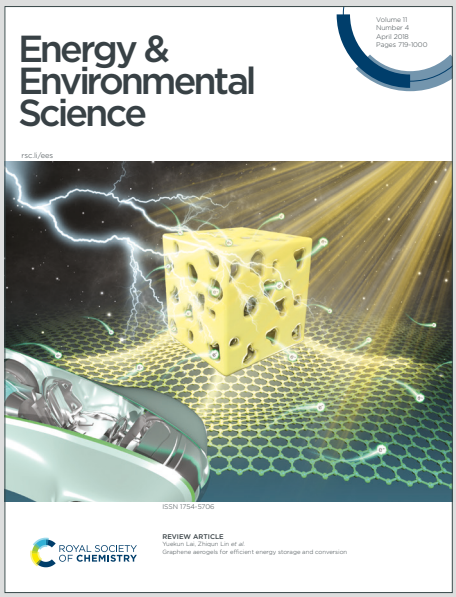

ROYAL SOCIETY OF CHEMISTRY

rsc.li/ees

View Article Online
DOI: 10.1039/D4EE03857F

Broader context

Aqueous Zn-V_2O_5 batteries, with their outstanding merits of intrinsic safety and high energy density, have garnered extensive attention for stationary energy storage. However, these batteries face critical challenges, particularly the severe dissolution of V_2O_5 cathode, which leads to capacity decay and structural degradation. This issue is exacerbated by the shuttling of dissolved V-O species, which not only diminishes cathode integrity but also triggers adverse side reactions at the Zn anode, such as zinc dendrite growth and hydrogen evolution reaction (HER), eventually accelerating battery failure. Although various previously reported modified strategies including structure modifications and electrolyte additives enable Zn-V_2O_5 batteries to realize excellent long-term cycling stability at ultra-high cycling rates from 5 C–50 C, the Zn-V_2O_5 batteries are usually unable to undergo stable cycling at the moderate rates (< 0.25-2 C). In this work, a developed polybenzimidazole (PBI) hydrogel electrolyte not only reduce the amount of free water by forming abundant hydrogen bonds but also minimize proton co-intercalation into V_2O_5 host, to suppress both V_2O_5 chemical dissolution and electrochemical dissolution simultaneously. Moreover, the PBI electrolyte also effectively prevents the crosstalk of $V_{10}O_{26}(OH)_2^{4-}$ between anode and cathode to enable durable high-areal-capacity Zn-V_2O_5 batteries at moderate cycling rates (< 2 C).

View Article Online
DOI: 10.1039/D4EE03857F

ARTICLE

Inhibiting cathode dissolution and shuttling of V-O species by a polybenzimidazole hydrogel electrolyte for durable high-areal-capacity Zn-V_2O_5 batteries

Received 00th January 20xx,
Accepted 00th January 20xx

DOI: 10.1039/x0xx00000x

Zeheng Lv,[a] Rong Tang,[a] Chenxi Sun,[a] Weiwei Meng,[b] Jin Yang,[a] Siyang Li,[a] Qilong Wu,[a] Minghao Zhang,[a] Jinbao Zhao,*[a] Yang Yang *[a]

Aqueous Zn-V_2O_5 batteries, renowned for their intrinsic safety and high energy density, hold significant promises for large-scale energy storage. Despite achieving impressive fast-charging performance, maintaining long-term cycling performance in practical Zn-V_2O_5 batteries with high areal capacities (> 2 mAh cm^{-2}) at moderate cycling rates (< 1 C) remains a formidable challenge due to aggravated cathode dissolution issues. Herein, a polybenzimidazole (PBI) hydrogel electrolyte is developed to suppress cathode dissolution and shuttling of dissolved V-O species simultaneously. Based on advanced characterizations including in-situ X-ray diffraction and electrochemical quartz crystal microbalance, the degradation mechanism of commercial V_2O_5 cathode is elucidated to both chemical dissolution, triggered by active water attack and electrochemical dissolution, induced by pH fluctuation following proton intercalation. Accordingly, the unique electron cloud density distributions of PBI chains not only reduce the amount of free water by forming abundant hydrogen bonds but also minimize proton co-intercalation by transporting Zn^{2+} selectively. Moreover, the PBI electrolyte also effectively prevents the crosstalk of polyvanadate ions through synergistic physical barrier and chemical adsorption effects. Therefore, the Zn-V_2O_5 battery using PBI electrolyte demonstrate one of the best low-rate cycling stabilities reported to date (~ 2 mAh cm^{-2} at 0.3 C over 300 cycles), verifying its feasibility.

Introduction

To address the depletion crisis of fossil fuels, the development of electrochemical energy storage technology is being pursued vigorously. Over the last decades, lithium-ion batteries (LIBs) have dominated the major power source markets for electric vehicles and portable electronics due to their sophisticated design and high energy density characteristics. However, LIBs may not be the sole option for emerging stationary energy storage application. Because the flammable organic electrolyte essential for LIBs poses an explosion risk, and the high cost of lithium-containing materials further hinders their extensive development.[1] Fortunately, aqueous Zn metal batteries (ZMBs) offer inherent advantages of high safety and low cost due to the use of inexpensive, air-stable aqueous electrolytes and high-energy Zn metal anodes (820 mAh g^{-1} and 5855 mAh cm^{-3}).[1-4] These features of ZMBs could potentially compensate for the weakness of LIBs and satisfy most of the key metrics required for alternative stationary energy storage systems.[5-7]

Generally, the energy densities of ZMBs are determined by the cathodes. Among various cathode candidates, including Prussian blue analogues, Mn and V-based oxides, sulfur-based materials and organic electrodes, V_2O_5 features a high theoretical capacity (589 mAh g^{-1}) and an appropriate layered structure for rapid ion intercalation, attracting ever-increasing attention.[8] However, the V_2O_5 cathode suffers from dissolution issues during cycling, resulting in unsatisfactory cycling stability due to the loss of active material. It is widely believed that V_2O_5 dissolution is induced by the attack of active water molecules in the electrolyte ($V_2O_5 + 3H_2O \rightarrow 2VO_2(OH)_2^- + 2H^+$), and the growing consensus on suppressing V_2O_5 dissolution lies in lowering the water activity.[9-13] Strategies to reduce surrounding coordinated water of the hydrated Zn^{2+} or the adsorbed water at cathode/electrolyte interface have been demonstrated to enhance the structural stability of V_2O_5 cathode during cycling.[9, 10, 12] This improvement can be attributed to the facilitated $[Zn(H_2O)_6]^{2+}$ desolvation behavior at the cathode/electrolyte interface, as V_2O_5 dissolution readily occurs in the presence of polar bound water.[12-14] Despite significant progress, most long-term cycling performance of Zn-V_2O_5 full cells is still achieved under high current rates (> 2 C),[2, 15] and the primary cathodic issues of V-O dissolution and capacity decay are easily masked by thousands of cycles at high current rates.[14] It should be noted that most electrochemical devices typically operate at modest current rates (0.2-2 C), thereby

[a] State Key Laboratory of Physical Chemistry of Solid Surfaces, State-Province Joint Engineering Laboratory of Power Source Technology for New Energy Vehicle, College of Chemistry and Chemical Engineering, Xiamen University, Xiamen, 361005, P. R. China. E-mail: jbzhao@xmu.edu.cn, yangyang419@xmu.edu.cn
[b] Key Laboratory of Functional Materials and Devices for Special Environments of CAS, Xinjiang Key Laboratory of Electronic Information Materials and Devices; Xinjiang Technical Institute of Physics & Chemistry of CAS, Urumqi 830011, P. R. China

Supplementary Information available: [details of any supplementary information available should be included here]. See DOI: 10.1039/x0xx00000x

View Article Online
DOI: 10.1039/D4EE03875J

eliminating the large gap between low-rate and high-rate cycling stability requires a more meticulous interface regulation approach. Very recently, He et al. proposed a zinc-permeable and hydrophobic interphase on vanadium oxide cathodes to restrain active material dissolution, enabling stable cycling for 200 cycles at 0.47 C.[11] However, its feasibility under high-areal-capacity conditions should be further validated. Specifically, higher areal capacities mean the adoption of high-loading cathodes, which not only face more serious dissolution issues but also trigger detrimental side reactions on the Zn metal anode owing to the shuttling of dissolved products.

To fundamentally address the dissolution issues of high-loading V_2O_5 cathodes, it is necessary to conduct a comprehensive study of their dissolution mechanism and the evolution of electrode structure and dissolved products. Based on theoretical calculations and various ex/in situ characterizations, we conclude that the dissolution process of V_2O_5 can be categorized into two representative types: chemical dissolution and electrochemical dissolution processes. The former is due to active water attacking the V-O bond, while the latter arises from the spontaneous reaction between V_2O_5 and interfacial OH^- resulting from proton intercalation (Fig. 1a).[8, 13, 14, 16] The dissolved $VO_2(OH)_2^-$ at the cathode/electrolyte interface will diffuse into the weakly acidic electrolyte and polymerize to form $V_{10}O_{26}(OH)_2^{4-}$, which then transfers to the anode through the concentration gradient. Meanwhile, the hydrogen evolution reaction (HER) on Zn metal anode causes a local increase of pH, triggering the disintegration of $V_{10}O_{26}(OH)_2^{4-}$ into $VO_2(OH)_2^-$ and the subsequent formation of insoluble $Zn_3V_2O_7(OH)_2{\cdot}nH_2O$ (ZVO). The accumulation of these irreversible products on the Zn surface not only consumes active materials but also passivates the anode interface, further exacerbating HER and dendrite growth, and potentially leading to internal short circuit of Zn-V_2O_5 batteries. Therefore, reducing water activity and constraining proton co-intercalation synergistically seem to be the ultimate route to minimize cathode dissolution in practical Zn-V_2O_5 batteries.[14, 17]

Actually, many cross-linked hydrogel electrolytes (or the so-called two-in-one electrolytes) possess the general features: (1) the activities of both water and proton could be reduced by the polar groups in hydrogel electroltyes,[18] (2) the polar groups in gel electrolytes would also adsorb the cation and anion ions, and the ordered distribution of cation/anion ions benefits to reducing the concentration gradient and side reactions near the surface of electrode,[19, 20] (3) the two-in-one electrolytes not only can be utilized to assemble flexible devices, but also can simplify the assembly process because the process of injecting liquid electrolyte can be removed.[21, 22] In this work, a polybenzimidazole (PBI) hydrogel electrolyte is developed to simultaneously suppress both chemical and electrochemical dissolutions of V_2O_5 and hinder the shuttling of $V_{10}O_{26}(OH)_2^{4-}$. Specifically, the imine (C=N) and amine (-NH-) sites in the molecular structure of PBI exhibit distinct electron cloud density (ECD) distributions (Fig. 1a and Fig. S1), leading to unique functions are as following: (1) by forming hydrogen bond networks with water molecules, the PBI electrolyte significantly reduces the amount of free water, decreasing chemical dissolution of V_2O_5 and HER on Zn metal anode, (2) the PBI electrolyte also shows selective binding abilities toward Zn^{2+} and H^+, enhancing rapid Zn^{2+} intercalation while minimizing proton co-intercalation, (3) the PBI electrolyte effectively blocks the shuttle effect of polyvanadate ions through physical barriers and chemical adsorption effect (Fig. 1a).[23-29] Based on the stabilization of V-O species throughout the entire battery, the PBI electrolyte enables one of the best low-rate cycling stabilities to date, achieving a high areal capacity of ~ 2 mAh cm^{-2} at a relatively low cycling rate of 0.3 C over 300 cycles.

Results and discussion

Through a facile phase inversion reaction, a PBI hydrogel membrane with dimensions of approximately 6 × 16.5 cm can be readily obtained (inset in Fig. 1a), demonstrating its feasibility for large-scale production. The dense and relatively rough surface formed by the fast exchange process between DMAC (N, N-dimethylacetamide) and deionized water is evident in the SEM image (Fig. S2). At the molecular level, the typical PBI structure exhibits a periodic arrangement of imidazole and benzene rings (inset in Fig. 1a), where the distinctive electron affinity of specific element results in -NH- and -N= groups carrying positive and negative charges, respectively (Fig. S1).[30] Besides, the FT-IR (Fourier transform infrared spectra) results (Fig. S3) and the evenly distributed C/N elements (Fig. S2) further confirm the successful preparation of the PBI membrane. The tensile tests indicate that the PBI hydrogel membrane can undergo both larger strain and higher tensile strength than the widely used GF separator (glass fiber, Fig. 1b). Through weighing the PBI hydrogel membrane before and after drying, the water content in PBI electrolyte is about 30.9%. Moreover, the high ionic conductivities of exceeding 1 mS cm^{-1} (Fig. S4) and stable ionic conductive behavior at various temperatures (Fig. 1c) of PBI hydrogel electrolyte ensure the rapid shuttling of Zn^{2+} ions between anode and cathode. Overall, the moderate mechanical property (Fig. S5 and S6) and excellent ionic conductivity enable PBI hydrogel membrane to be a feasible two-in-one separator/electrolyte for ZMBs.

By carefully comparing the FT-IR characteristic peaks of H_2O, dry PBI membrane and PBI-H_2O (water-containing PBI membrane), obvious shifts of both O-H stretching modes (bulk, cluster and isolated H_2O) and the C=N groups in PBI-H_2O can be observed (Fig. 1d and e, Fig. S3 and S7-S9), implying the potential interaction between water molecules and the pyridine N in PBI chains.[31] Abundant hydrogen bonds would exist in PBI-H_2O as the positive hydrogen end in H_2O is prone to be adsorbed by the negative -N=, and the oxygen end in H_2O would interact with the -NH- when a water molecule approaching PBI until reaching a steady state (Fig. 1f and g). This indicates an underlying interaction between PBI chain and free water molecule, also inhibiting proton reactivity in the PBI hydrogel. Accordingly, the linear sweep voltammetry (LSV, Fig. 1h) tests show the lower HER rate and higher HER overpotential for the PBI-Zn (the Zn metal was coated with PBI hydrogel for testing) while compare to the bare Zn. In-situ DEMS (differential electrochemical mass spectroscopy) measurements further demonstrate that the HER rate of Zn||Zn symmetrical battery using PBI hydrogel electrolyte is almost negligible and substantially lower than that with liquid 3 M $Zn(OTF)_2$ quantitatively (Fig. 1i and j). Consequently, the

View Article Online
DOI: 10.1039/D4EE03857F

effective suppression of water activity in PBI hydrogel is expected to alleviate the V_2O_5 dissolution and improve the cycling stability of Zn-V_2O_5 batteries.

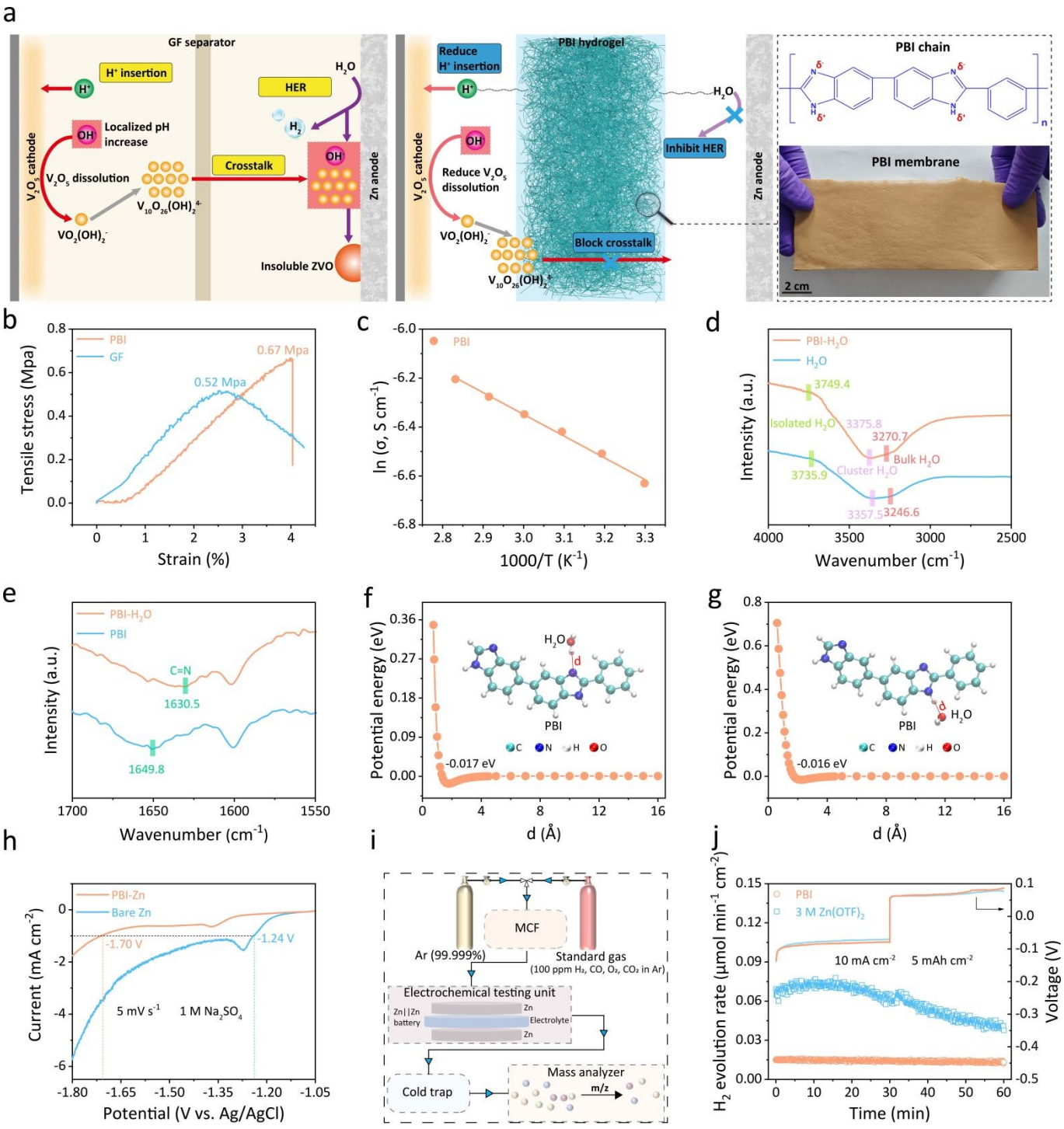

Fig. 1 V_2O_5 dissolution process and the reduced water activity in PBI hydrogel electrolytes. (a) Comparison of different V_2O_5 dissolution behaviors with GF (glass fiber) separator and PBI hydrogel. (b) Stress-strain curves of GF separator and PBI hydrogel. (c) Arrhenius plots of the ionic conductivities for PBI hydrogel electrolyte. FT-IR results of (d) PBI-H_2O and H_2O, and (e) PBI-H_2O and PBI. Evolutions of potential energies with different distances between (f) the imine (C=N) site in PBI and H_2O, (g) the amine (-NH-) site in PBI and H_2O. (h) LSV test results of Bare Zn and PBI-Zn (the Zn metal was coated with PBI hydrogel for testing) in 1 M Na_2SO_4 at 5 mV s^{-1}. (i) Illustration of in-situ DEMS measurement. (j) In-situ DEMS measurement results of Zn||Zn symmetrical batteries using liquid 3 M $Zn(OTF)_2$ (zinc trifluoromethanesulfonate) and PBI hydrogel electrolytes.

To ensure significant practicability, commercial V_2O_5 powder (Fig. S10), which eliminates the need for complex synthesis process, was directly used as the active material in this study. It is generally accepted that the good cycling performance of pristine V_2O_5 cathode can only be maintained after rational pre-activation to a certain extent.[8] Therefore, a customized

View Article Online
DOI: 10.1039/D4EE03875E

electrochemical activation procedure is designed, targeting a reversible capacity reaching 350 mAh g^{-1} as the standard level (Fig. S11). After the pre-activation process, the color changes of GF/PBI separators were observed. A noticeable brown color appearing on the cathodic side and an even deeper color on the anodic side of GF (Fig. 2a), but there is almost no color change on the anodic PBI (Fig. S12), suggesting the occurrence of V_2O_5 dissolution and the blocked shuttling of dissolved V-O species in PBI. During subsequent cycling, the higher reversible capacity and more prominent capacity increase trend of the Zn||V_2O_5 battery with 3 M $Zn(OTF)_2$ may be attributed to the larger amount of protons co-intercalation resulting from the higher water reactivity in the liquid electrolyte (Fig. 2a and b). And the consequent capacity decay and battery failure (Fig. S13 and S14, Fig. 2b) are caused by V_2O_5 dissolution and the formation of passivation products (ZVO) and/or zinc dendrites.[8, 32] On the contrary, the reduced water activity in PBI electrolyte promotes the Zn||V_2O_5 full cells to retain a high areal capacity of ~ 2 mAh cm^{-2} at the low rate of 0.3 C (0.2 A g^{-1}, ~ 1.0 mA cm^{-2}) after 300 cycles (Fig. 2a and Fig. S15). As shown in Fig. 2b (Fig. S16), a considerable capacity retention of 88.2% can be maintained over 1000 cycles at a moderate cycling rate of 1.7 C (1 A g^{-1}, ~ 5.0 mA cm^{-2}), which is superior to the electrochemical performance of many previously reported V-based materials (Fig. 2g and Table S1).[5, 12, 33-40] Interestingly, the capacity decay of Zn||V_2O_5 full cells with PBI electrolyte is almost negligible when the rate is increased from 0.3 to 1.7 C (Fig. 2a and b), illustrating the good rate capability of V_2O_5 cathode after the pre-activation (Fig. S17-S20). It should be noted that the thickness of the Zn foil used in our work is 100 μm and the depth of discharge (DOD) of the Zn anode is estimated to be ~ 3.4%. Besides, the pouch cells were also fabricated to further examine the feasibility of PBI electrolytes in Zn-V_2O_5 batteries (Fig. S21-S26). As a result, the Zn||V_2O_5 pouch cell can cycle with ~ 3.8 mAh cm^{-2} for 25 cycles at 1.7 C, demonstrating the practicality of the Zn-V_2O_5 batteries with PBI electrolytes. To analyze the deposition of the dissolved V-O species on Zn anode quantitatively, inductively coupled plasma spectrometer (ICP) was utilized to determine the V^{5+} content of dissembled Zn metal electrodes after 10 cycles at 0.2 C. As shown in Fig. S27, the V^{5+} in Zn electrode with PBI is only one tenth of that with 3 M $Zn(OTF)_2$, confirming the limited V-O species crosstalk between cathode and anode by using PBI electrolyte. Furthermore, a mixed electrolyte including 3 M $Zn(OTF)_2$ and 0.003 M $V_{10}O_{26}(OH)_2^{4-}$ aqueous solution (denoted as 3 M $Zn(OTF)_2$/V) (Fig. S28) was employed to fabricate Zn||Zn symmetrical batteries to simulate the durability of Zn metal anodes in V-containing environment. During 50 cycles test procedure in Fig. 2d, the Zn||Zn symmetrical cell can cycle stably with PBI/V (PBI electrolyte containing 3 M $Zn(OTF)_2$/V), but quickly fail with 3 M $Zn(OTF)_2$/V after only 10 cycles. Moreover, the Zn||Zn symmetrical cell not only can cycle for about 400 h at 1 mAh cm^{-2} and 1 mA cm^{-2} with both PBI/V and the PBI electrolyte containing the commonly employed 2 M $ZnSO_4$, but also can reversibly cycle at the higher capacities of 3 and 5 mAh cm^{-2} with PBI/V (Fig. S29-S32). Additionally, the distinct V^{5+} concentration difference for Zn metal in different electrolytes reveals that V-O species dramatically deteriorate the reversibility of Zn anode, while the PBI electrolyte could absorb and stabilize V-O species to restrain side reactions on Zn metal surface (Fig. 2c). Meanwhile, V_2O_5 dissolution would also induce the self-discharge concern of Zn||V_2O_5 battery.[9, 12] Compare to the counterpart in Fig. 2e, the improved self-discharge effect of Zn||V_2O_5 battery in Fig. 2f illustrates the suppressed spontaneous chemical dissolution of V_2O_5 can be achieved by PBI electrolyte. Therefore, the PBI electrolyte can simultaneously suppress both V_2O_5 dissolution and the shuttling of V-O species to prolong the lifespan of Zn-V_2O_5 batteries.

View Article Online
DOI: 10.1039/D4EE03855E

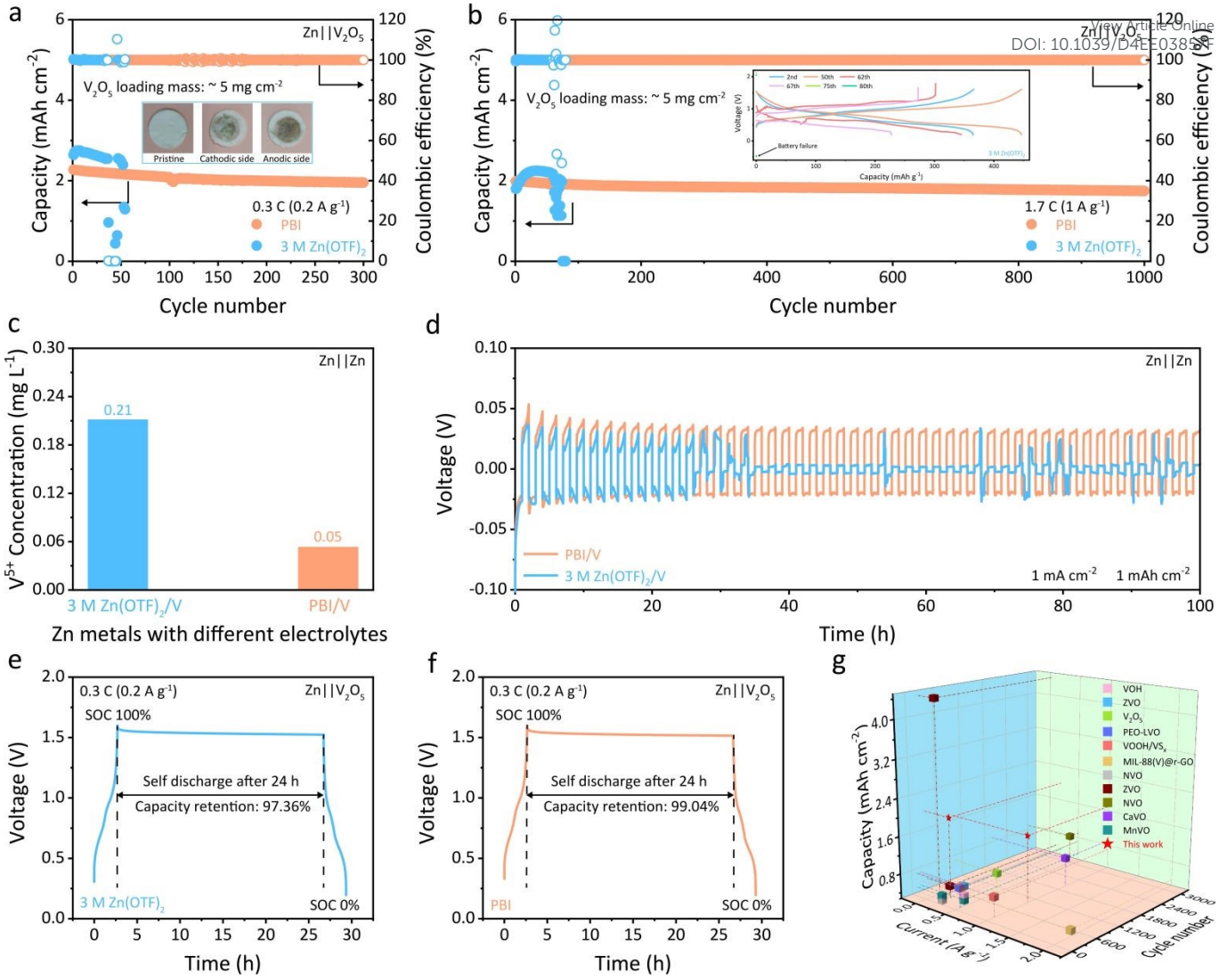

Fig. 2 Improved electrochemical performances of Zn||V_2O_5 batteries using PBI hydrogel electrolytes. Cycling performances of Zn||V_2O_5 batteries with 3 M $Zn(OTF)_2$ and PBI hydrogel electrolytes at (a) 0.3 C and (b) 1.7 C. The insets in Fig. 2a and b are GF separators before and after activation, and the discharge-charge curves for Zn||V_2O_5 batteries with 3 M $Zn(OTF)_2$, respectively. (c) The ICP results of the V^{5+} content for the dissembled Zn metals in Zn||Zn batteries with 1 mA cm^{-2} and 1 mAh cm^{-2} after 10 cycles. (d) Cycling performances of Zn||Zn batteries with 1 mA cm^{-2} and 1 mAh cm^{-2}. The mixed electrolyte for the above Zn||Zn batteries is composed of 3 M $Zn(OTF)_2$ and the as-prepared 0.003 M $V_{10}O_{26}(OH)_2^{4-}$ aqueous solution with a volume ratio of 9:1. Self-discharge test results for Zn||V_2O_5 batteries with (e) 3 M $Zn(OTF)_2$ and (f) PBI hydrogel electrolytes. (g) Cycling stabilities comparisons of Zn||V_2O_5 batteries with PBI hydrogel electrolyte and the other reported V-based materials.

Clarifying the shuttling pathway of V-O species in battery is necessary for further identifying the failure mechanism of V_2O_5 cathode. Firstly, the saturated V-O containing solution prepared by immersing excessive V_2O_5 powder into 3 M $Zn(OTF)_2$ over two months was analyzed by ^{51}V nuclear magnetic resonance (NMR). As shown in Fig. 3a, a pronounced peak at around -520.6 ppm is assigned to $V_{10}O_{26}(OH)_2^{4-}$, confirming the main constitute for the dissolved V-O species is $V_{10}O_{26}(OH)_2^{4-}$. And the initial dissolved $VO_2(OH)_2^-$ at the cathode/electrolyte interface undergoes a spontaneous polymerization evolution in the bulk electrolyte.[41] Moreover, the as-prepared $V_{10}O_{26}(OH)_2^{4-}$ aqueous solution (Fig. S28) was exploited to further verify the anti-penetration ability of the PBI membrane. As depicted in Fig. 3d, the color of the right solution is deepened more quickly while using GF separator. And the corresponding ICP results in Fig. 3e also quantitatively illustrate the $V_{10}O_{26}(OH)_2^{4-}$ is easier to diffuse through GF. This $V_{10}O_{26}(OH)_2^{4-}$ anti-penetration effect of PBI could be further assessed through ESP simulations. In Fig. 3c, when the $V_{10}O_{26}(OH)_2^{4-}$ is polymerized near the PBI electrolyte, the negative potential energy of -0.196 eV indicates that the positively charged -NH- groups of PBI could adsorb $V_{10}O_{26}(OH)_2^{4-}$ significantly (Fig. 3b), explaining $V_{10}O_{26}(OH)_2^{4-}$ could hardly approach the surface of Zn anode through the PBI membrane. Additionally, many other hydrogel electrolytes with polar groups may also possess the similar chemical adsorption function. However, the as-prepared widely studied polyacrylamide (PAM) hydrogel shows an inferior practical anti-penetration effect on the V-O species (Fig. S33-35), which may could be attributed to the high water compatibility of PAM cause the V-O species easily move with water molecules through the PAM hydrogel. This result reflects the PBI electrolyte possesses the distinctive block effect on the shuttling of $V_{10}O_{26}(OH)_2^{4-}$. In addition, the function of suppressing V_2O_5 dissolution for PBI chains are also revealed by advanced in-situ

View Article Online
DOI: 10.1039/D4EE03857F

electrochemical quartz crystal microbalance (EQCM) measurements (Fig. 3f). Over time, the frequencies of the V_2O_5 electrode increase continuously when using conventional polyvinylidene fluoride (PVDF) binder at 0.5 mV s^{-1} (Fig. 3g and h), but which decrease firstly and then increase to a value that lower than the initial while using PBI binder. This result implies that the V_2O_5 dissolution loss with PVDF is higher than the weight increase associated with ion intercalation, and PBI can effectively suppress the V_2O_5 dissolution. Interestingly, the V_2O_5 electrodes with both PVDF and PBI binders display reversible mass evolutions at a higher scan rate of 5 mV s^{-1} (Fig. 3i and j), indicating that V_2O_5 dissolution is effectively masked at a relatively high cycling rate, which is consistent with the previously established understanding in the academic community.[11-14, 32, 42]

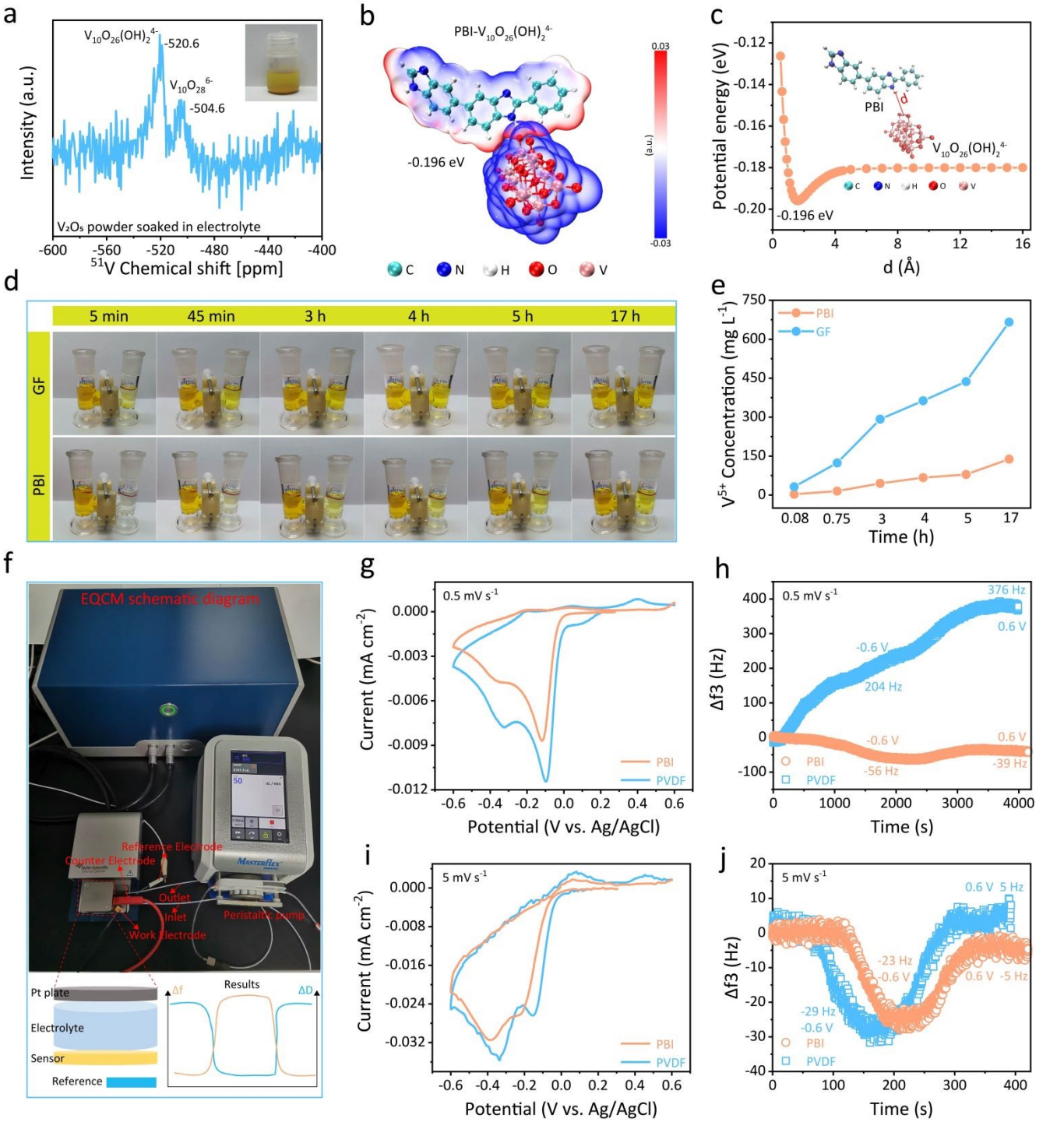

Fig. 3 Quantitative analysis of V-O species dissolution and shuttling. (a) ^{51}V NMR result of the as-prepared saturated V-O containing solution. (b) ESP result of PBI-$V_{10}O_{26}(OH)_2^{4-}$. (c) Evolution of potential energies with different distances between PBI and $V_{10}O_{26}(OH)_2^{4-}$. (d) Visual penetration processes of the as-prepared $V_{10}O_{26}(OH)_2^{4-}$ solution, and (e) the corresponding ICP results for GF separator and PBI membrane. (f) Optical photo of the EQCM device. Results of Cyclic voltammetry test for V_2O_5 electrode with PVDF and PBI binders at (g) 0.5 and (i) 5 mV s^{-1}, and (h and j) the corresponding in-situ EQCM measurement results.

Although the dissolution of V_2O_5 induced by active water had been studied in previous literature, the specific relationship between dissolution process and structural evolution of V_2O_5 remains unclear. To elucidate this point, in-situ XRD (X-ray diffraction) measurements were conducted. At the beginning of discharge process (Fig. S36), the characteristic peaks of V_2O_5 (JCPDS No. 41-1426) shift to either higher or lower degree, corresponding to the layered structural evolution derived from the co-intercalation of $[Zn(H_2O)_x]^{2+}$ and protons. The insertion of $[Zn(H_2O)_x]^{2+}$ also causes interlayer contraction of V_2O_5 host due to the interlayer electrostatic interaction between Zn^{2+} and V_2O_5 crystal lattice.[43-45] Besides, the appearance of new peaks at ~ 6.6°, 13.2°, 19.8° and 33.1° suggests the formation of layered $Zn_xV_2O_5{\cdot}nH_2O$ phases with a set of (00l) planes (l = 1-7), leading to the increased interlayer distance of V_2O_5 from 4.4 to 13.4 Å (Fig. S36b-e and h-k).[46] By comparing the phase evolutions of $Zn_xV_2O_5{\cdot}nH_2O$ and the (001) peak shifts of V_2O_5 host in both electrolytes (Fig. S36d and j), it can be observed that the intensities of $Zn_xV_2O_5{\cdot}nH_2O$ reflections with 3 M $Zn(OTF)_2$ increase more quickly, with a more pronounced deviation in (001) peak. This indicates that the intercalation of a greater number of protons stemming from the relatively higher-active water in 3 M $Zn(OTF)_2$, could alleviate the electrostatic adsorption of divalent inserted Zn^{2+} and O in V_2O_5, thereby accelerating the initial $[Zn(H_2O)_x]^{2+}$ intercalation kinetics.[43] Additionally, during the entire discharge and charge processes, the evolutions of characteristic peaks with PBI including (001), (101), (110) and (301) appear smoother compared to those with 3 M $Zn(OTF)_2$. This may indicate that the crystalline structure of V_2O_5 with PBI electrolyte is less susceptible to degradation by active water, leading to improved structural stability of V_2O_5.

Furthermore, three additional peaks at approximately 12.3°, 30.1° and 34.0° appearing during the second cycle (Fig. 4b, d, g and i) are assigned to the ZVO by-product, which is generated by the reaction between dissolved $VO_2(OH)_2^-$ and Zn^{2+}. This observation suggests the occurrence of V_2O_5 electrochemical dissolution, which is triggered by pH disturbances at the cathode/electrolyte interface.[8, 11, 16] As cycling continues, the intensities of ZVO peaks remain relatively unchanged from the 8th cycle with PBI but become less noticeable with 3 M $Zn(OTF)_2$, which seems inconsistent with the higher proton insertion tendency due to the higher water reactivity in 3 M $Zn(OTF)_2$. It is hypothesized that the growth of ZVO on electrode surface relies on a dissolution-precipitation reaction. Initially, ZVO peaks may not be observed due to the low initial concentration of $VO_2(OH)_2^-$. Meanwhile, once the interfacial concentration of $VO_2(OH)_2^-$ becomes insufficient to form ZVO, the concentration gradient drives the diffusion of $VO_2(OH)_2^-$ into the bulk electrolyte. Therefore, the prominent ZVO peaks in the presence of PBI electrolyte indicate that the diffusion of $VO_2(OH)_2^-$ is restrained by PBI membrane, and the $VO_2(OH)_2^-$ is concentrated near the electrode/electrolyte interface. Moreover, the release of H^+ following ZVO formation regulates the cathode/electrolyte interfacial pH to a value that inhibits further V_2O_5 electrochemical dissolution.[8] During the 4th cycle, another by-product of $Zn_x{\cdot}(CF_3SO_3)_y(OH)_{2x-y}{\cdot}nH_2O$ (ZSO), typically formed in alkaline environments, is observed with 3 M $Zn(OTF)_2$ (Fig. 4b) but is almost absent with PBI (Fig. 4g). This reveals that the more serious pH fluctuation occur in 3 M $Zn(OTF)_2$, resulting from increased proton insertion. The inhibited proton insertion in the presence of PBI can be further understood through the ESP results. As shown in Fig. 4k, a considerable binding energy of -0.236 eV demonstrates that PBI chain can significantly restrict the free movement of H^+ (Fig. 4l), which may be associated with suppressed proton insertion into V_2O_5 (Fig. S37).

As the activation progresses, the pristine V_2O_5 evolves into a mixture of V_2O_5 and $V_2O_5{\cdot}nH_2O$ phases gradually (Fig. 4d and i).[16] This phase transformation is accompanied by a decrease in the crystallinity of V_2O_5, primarily due to the attack by active H_2O molecules (Fig. 4c, e, h and j). According to the interaction depicted in Fig. S38, it is predicted that the O and H atoms in H_2O would interact with the V and O atoms in V_2O_5, respectively. The obvious charge accumulation surrounding the O in H_2O and the charge depletion near the V in V_2O_5 are caused by differences in electronegativity (Fig. 4n). This leads to a partial transfer of delocalized electrons from the V in V_2O_5 to the O in H_2O (Fig. 4o), corresponding to the tendency of V_2O_5 to undergo chemical dissolution due to the decreased bond energy of V-O bond in V_2O_5 caused by the active water attack. When a PBI chain was introduced (Fig. S39), the electrons around pyridine N in PBI tend to redistribute as the electronegativity of O is higher than N (Fig. 4p). This redistribution of electron density renders the O in H_2O more negative, thereby makes it harder for these O atoms to rip electrons away from V-O bonds in V_2O_5. As a result, the delocalized electrons derived from V-O bonds in V_2O_5 are more accumulated near V but less around the O in H_2O (Fig. 4q), illustrating that PBI could mitigate part of electrostatic binding force from free water and V-O bonds to improve the chemical stability of V_2O_5 in aqueous environment.

The complete evolution routes for V_2O_5 dissolution and the shuttling of dissolved V-O species are concluded in Fig. 4m. The process begins with spontaneous chemical dissolution (1) when V_2O_5 contacts with the electrolyte. Following this, H_3O^+ intercalates into V_2O_5 host, generating an equivalent amount of OH^- (2). Both the formation of ZSO (4) and electrochemical dissolution reactions of V_2O_5 (3) consume OH^-, with the later process occurring before the former. It is worth noting that the main forms of V-O ionic species are determined by their concentration and existing pH environment.[8, 41] If the diffusion of dissolved $VO_2(OH)_2^-$ is not effectively blocked, V_2O_5 continues to dissolve at a relatively high rate and the aggregated $VO_2(OH)_2^-$ may polymerize to generate $V_{10}O_{26}(OH)_2^{4-}$ (5) near the bulk electrolyte as pH decreases and V^{5+} concentration increases. Alternatively, sufficient $VO_2(OH)_2^-$ will combine with Zn^{2+} to form ZVO (6) on the surface of V_2O_5. It is reasonable that the efficient block of $VO_2(OH)_2^-$ diffusion will expedite the formation of a ZVO protective layer on cathode surface. The released H^+ during (1) and (6) will help to alleviate both ZSO growth and V_2O_5 dissolution. Meanwhile, the pH increase caused by the inevitable cathodic H_3O^+ intercalation and anodic HER should induce the depolymerization of $V_{10}O_{26}(OH)_2^{4-}$ back into $VO_2(OH)_2^-$ at the surfaces of both V_2O_5 cathode (7) and Zn anode (8) simultaneously. The generated OH^- and $VO_2(OH)_2^-$ may then cause the formation of ZSO and/or ZVO precipitates onto V_2O_5 (4 and 6) and Zn metal (9 and 10). The concomitant release of H^+ following ZVO generation and $V_{10}O_{26}(OH)_2^{4-}$ depolymerization would exacerbate side reactions at Zn metal anode side. Therefore, the PBI electrolyte, which effectively reduces proton intercalation and blocks

View Article Online
DOI: 10.1039/D4EE03857F

$V_{10}O_{26}(OH)_2^{4-}$ crosstalk, plays a crucial role in improving the cycling stability of Zn-V_2O_5 battery.

$$V_2O_5 + 3H_2O \rightarrow 2VO_2(OH)_2^- + 2H^+ \quad (1)$$

$$2H_2O \rightarrow H_3O^+ + OH^- \quad (2\text{-}1)$$

$$V_2O_5 + xH_3O^+ + xe^- \rightarrow H_xV_2O_5 \cdot xH_2O \quad (2\text{-}2)$$

$$V_2O_5 + H_2O + 2OH^- \rightarrow 2VO_2(OH)_2^- \quad (3)$$

$$xZn^{2+} + yCF_3SO_3^- + (2x\text{-}y)OH^- + nH_2O \rightarrow Zn_x(CF_3SO_3)_y(OH)_{2x\text{-}y} \cdot nH_2O\ (ZSO)\downarrow \quad (4)$$

$$10VO_2(OH)_2^- + 6H^+ \rightarrow V_{10}O_{26}(OH)_2^{4-} + 12H_2O \quad (5)$$

$$2VO_2(OH)_2^- + 3Zn^{2+} + 3H_2O \rightarrow Zn_3V_2O_7(OH)_2 \cdot nH_2O\ (ZVO)\downarrow + 4H^+ \quad (6)$$

$$V_{10}O_{26}(OH)_2^{4-} + 12H_2O \rightarrow 10VO_2(OH)_2^- + 6H^+ \quad (7)$$

$$2H_2O + 2e^- \rightarrow H_2 + 2OH^- \ (pH\uparrow) \quad (8\text{-}1)$$

$$V_{10}O_{26}(OH)_2^{4-} + 12H_2O \rightarrow 10VO_2(OH)_2^- + 6H^+ \quad (8\text{-}2)$$

$$xZn^{2+} + yCF_3SO_3^- + (2x\text{-}y)OH^- + nH_2O \rightarrow Zn_x(CF_3SO_3)_y(OH)_{2x\text{-}y} \cdot nH_2O\ (ZSO)\downarrow \quad (9)$$

$$2VO_2(OH)_2^- + 3Zn^{2+} + 3H_2O \rightarrow Zn_3V_2O_7(OH)_2 \cdot nH_2O\ (ZVO)\downarrow + 4H^+ \quad (10)$$

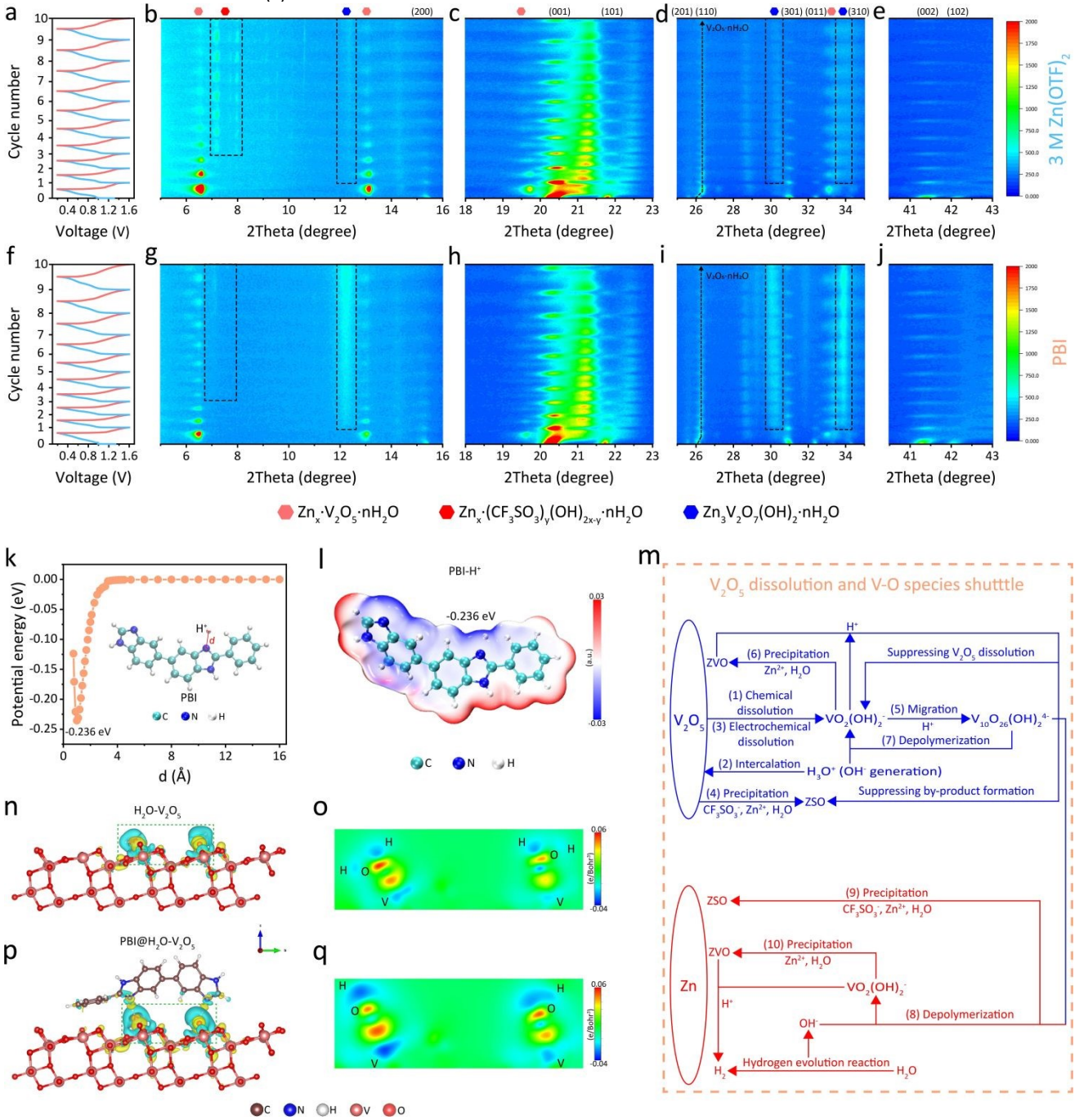

Fig. 4 Electrochemical evolution processes of the pristine V_2O_5 cathodes with different electrolytes and the interaction between V_2O_5 and H_2O. Discharge-charge curves of Zn||V_2O_5 batteries with (a) 3 M $Zn(OTF)_2$ and (f) PBI hydrogel electrolytes during the initial ten cycles. The corresponding in-situ XRD results of Zn||V_2O_5 batteries with (b-e) 3 M $Zn(OTF)_2$ and (g-j) PBI hydrogel electrolytes. (k) Evolution of potential energies with different distances between PBI and H^+. (l) ESP result of PBI-H^+. (m) Schematic illustrations of V_2O_5 dissolution and the dissolved V-O species shuttle mechanisms. Charge density difference of (n) H_2O-V_2O_5 and (p) PBI@H_2O-V_2O_5. Yellow and blue-green regions represent charge accumulation

and depletion, respectively. The Electron densities of (o) H_2O-V_2O_5 and (q) PBI@H_2O-V_2O_5 correspond to the green boxes in (n) and (p), respectively. Blue and red areas represent electron depletion and accumulation, respectively.

View Article Online
DOI: 10.1039/D4EE03857F

In addition to reducing proton insertion and V_2O_5 dissolution, the influence of suppressed water activity in PBI electrolyte on the cycling stability of V_2O_5 was further investigated using hydrated V_2O_5 electrodes after the pre-activation procedure (Fig. S11). Inspired by previous reports, the increase in intensity of the $Zn_x{\cdot}V_2O_5{\cdot}nH_2O$ reflections is closely related to the zinc content.[43] Compared to the relative intensities in liquid electrolyte (Fig. 5b and c), the narrower and stronger $Zn_x{\cdot}V_2O_5{\cdot}nH_2O$ peaks appearing with PBI (Fig. 5f and g) reflect a more pronounced $[Zn(H_2O)_x]^{2+}$ intercalation and higher crystallinity of V_2O_5 host. Similarly, the broadening phenomenon observed in the (001) and $V_2O_5{\cdot}nH_2O$ reflections (Fig. 5b and f), also suggests that the structural stability of V_2O_5 is inferior in 3 M $Zn(OTF)_2$. Interestingly, with $[Zn(H_2O)_x]^{2+}$ insertion, the (001) plane of V_2O_5 initially undergoes structural contraction due to electrostatic interaction between divalent Zn^{2+} and lattice O in V_2O_5. Subsequently, the interlayer distances of V_2O_5 gradually recover to nearly pristine states as the $Zn_x{\cdot}V_2O_5{\cdot}nH_2O$ phases appear (Fig. 5b and f, Fig. S40), implying that the $Zn_x{\cdot}V_2O_5{\cdot}nH_2O$ phase could help the V_2O_5 host to withstand repeated $[Zn(H_2O)_x]^{2+}$ intercalation/de-intercalation processes.

Additionally, to eliminate the possible inconsistencies introduced by the electrochemical activation, water pre-intercalation $V_2O_5{\cdot}1.6H_2O$ (JCPDS No. 40-1296) was synthesized via hydrothermal reaction (Fig. S41) to further verify different ion storage behaviors with 3 M $Zn(OTF)_2$ and PBI electrolytes (Fig. 5i-k and m-o).[47] The interlayer distances of $V_2O_5{\cdot}1.6H_2O$ enlarge firstly and then decrease during discharge (Fig. 5j and n, Fig. S42). This can be explained that the interlayer water pillar might overcome the initial electrostatic interaction of Zn^{2+} and $V_2O_5{\cdot}1.6H_2O$ host, but the continuous increased Zn^{2+} content force the interlayer structure of $V_2O_5{\cdot}1.6H_2O$ to be contracted. Similarly, the smooth changes of (001) peak could be attributed to the favorable interlayer buffering effect stemming from the $Zn_x{\cdot}V_2O_5{\cdot}nH_2O$ phases (Fig. 5j and n), and the higher relative intensities of $Zn_x{\cdot}V_2O_5{\cdot}nH_2O$ further confirm PBI can promote $[Zn(H_2O)_x]^{2+}$ intercalation (Fig. 5k and o), contributing to the higher cycling stability of Zn||$V_2O_5{\cdot}1.6H_2O$ battery using PBI electrolyte (Fig. S43). Besides, after fully charging, the irreversible residual interlayer water and Zn^{2+} ions cause the interlayer spaces of $V_2O_5{\cdot}1.6H_2O$ to be larger than the pristine state (Fig. S42), which may be beneficial for subsequent ion intercalation (Fig. S44).

Therefore, it can be concluded that the restrained water reactivity in PBI can not only promote $[Zn(H_2O)_x]^{2+}$ intercalation but also diminish V_2O_5 cathode degradation. This can be speculated from two aspects: the co-intercalation of H_3O^+ and $[Zn(H_2O)_x]^{2+}$, and the $[Zn(H_2O)_6]^{2+}$ desolvation process.[14, 39] Both binding energies of PBI-Zn^{2+} (-0.039 eV, Fig. 5d) and PBI-$[Zn(H_2O)_6]^{2+}$ (-0.035 eV, Fig. 5h) are lower than PBI-H^+ (-0.236 eV), highlighting that the PBI possesses the characteristics of higher Zn^{2+} selectivity. In addition, the ESP results of PBI-Zn^{2+} (Fig. S45) and PBI-$[Zn(H_2O)_6]^{2+}$ (Fig. S46) evidence PBI chain can bind with H_2O to offset part of interactions derived from Zn^{2+} and the solvated H_2O to weaken the solvation energy of $[Zn(H_2O)_6]^{2+}$. Moreover, the solvated water molecules in $[Zn(H_2O)_6]^{2+}$ show a prominent interaction with V_2O_5 through H in $[Zn(H_2O)_6]^{2+}$ and O in V_2O_5 (Fig. 5l). As shown in Fig. 5p, the isolated solvated water molecules with high polarity can significantly attack V_2O_5 and aggravate V_2O_5 dissolution subsequently, and the exotic divalent Zn^{2+} cations can spontaneously interact with the negative O in V_2O_5 to decrease the V-O bond energy, as well. Nevertheless, the weak solvation effect of $[Zn(H_2O)_6]^{2+}$ resulting from the PBI chain could reasonably facilitate the $[Zn(H_2O)_6]^{2+}$ desolvation reaction to improve the Zn^{2+} intercalation kinetics, and the V_2O_5 chemical dissolution is expected to be alleviated when the polar solvated water were bound by PBI chain.[10, 17, 48]

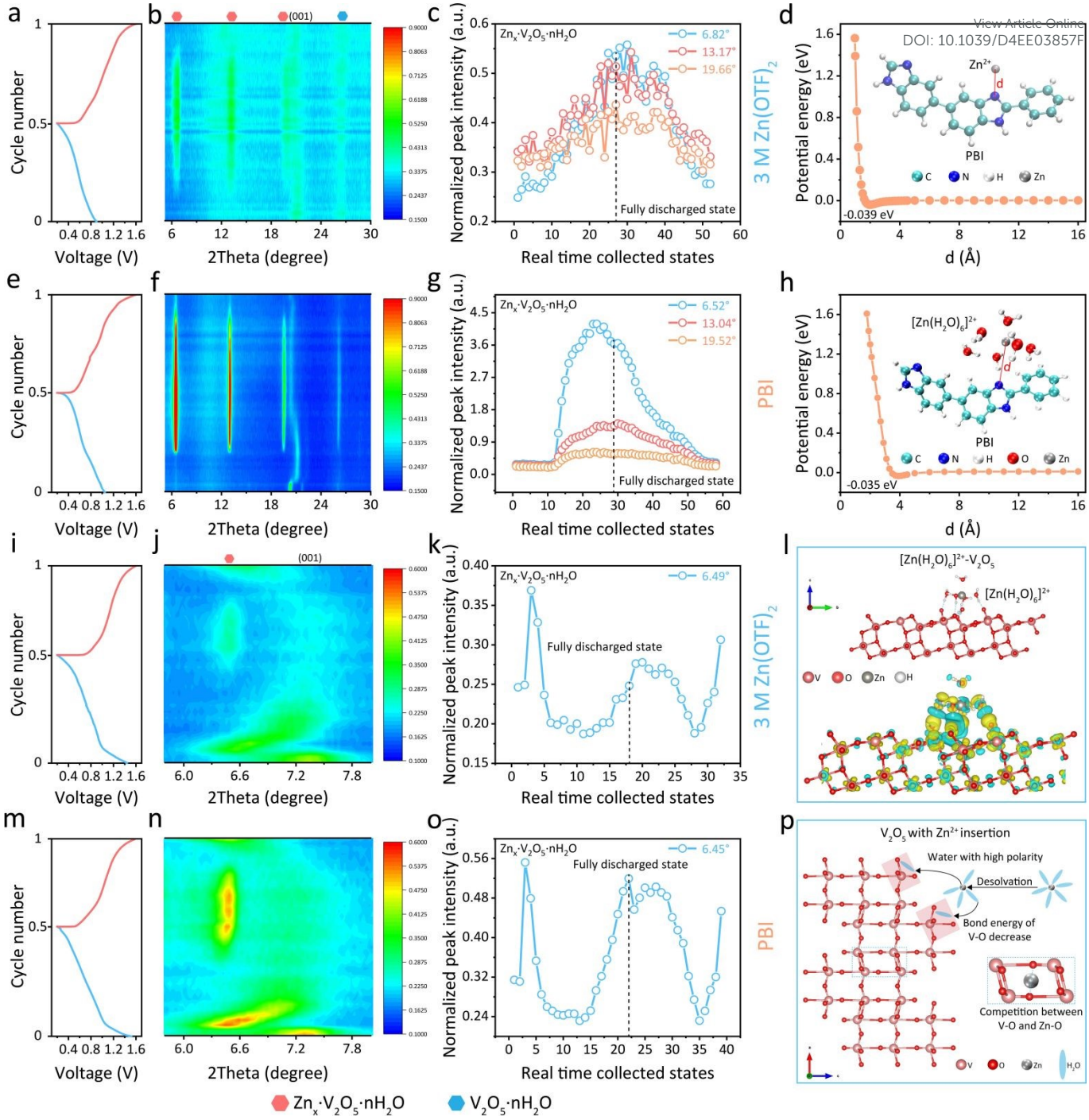

Fig. 5 Electrochemical evolution processes of the activated hydrated V_2O_5 and V_2O_5·1.6H_2O cathodes with different electrolytes and the interaction between V_2O_5 and $[Zn(H_2O)_6]^{2+}$. Discharge-charge curves of the activated hydrated V_2O_5 cathodes with (a) 3 M $Zn(OTF)_2$ and (e) PBI hydrogel electrolyte during the initial cycle. The corresponding normalized in-situ XRD results with (b and c) 3 M $Zn(OTF)_2$ and (f and g) PBI hydrogel electrolyte. Discharge-charge curves of the V_2O_5·1.6H_2O cathodes with (i) 3 M $Zn(OTF)_2$ and (m) PBI hydrogel electrolyte during the initial cycle. The corresponding normalized in-situ XRD results with (j and k) 3 M $Zn(OTF)_2$ and (n and o) PBI hydrogel electrolyte. The normalized intensities of all in-situ XRD results are figured out based on the loading mass of V_2O_5 and the diffraction intensities of stainless-steel current collectors. Evolutions of potential energies with different distances between (d) PBI and Zn^{2+}, (h) PBI and $[Zn(H_2O)_6]^{2+}$. (l) Charge density difference of $[Zn(H_2O)_6]^{2+}$-V_2O_5. Yellow and blue-green regions represent charge accumulation and depletion, respectively. (p) Possible interaction between V_2O_5 and the solvated water molecules, and the competitive interaction between Zn-O and V-O in the interlayer space of V_2O_5.

Conclusions

In general, the prepared PBI hydrogel electrolyte can reduce water activity by form hydron bond with H_2O, which help V_2O_5 to withstand the attack from active water molecules. The theoretical calculation results suggest PBI can not only restrain the free movement of proton, but also retard a part of interaction between V_2O_5 and water molecules. Additionally, the high Zn^{2+} selectivity of PBI chain enables dominant

$[Zn(H_2O)_x]^{2+}$ intercalation and suppressed proton insertion simultaneously, leading to the suppression of V_2O_5 dissolution. Moreover, the shuttling of the dissolved V-O species can be blocked by the polar group of -NH- in PBI, thereby, the low-current-density (< 2 C) cycling stability of Zn||V_2O_5 batteries can be improved by PBI electrolyte. More importantly, through a series of characterizations, the underlying mechanisms of complicated V-O species dissolution/shuttle in Zn-V_2O_5 batteries are revealed, assisting the improvements of practical electrochemical performances of the Zn-V_2O_5 full cells.

Author contributions

Conceptualization: Z. L. and Y. Y. Experimental design and investigation: Z. L. Data analyses: Z. L., R. T., C. S., W. M., J. Y., S. L., Q. W., M. Z., J. Z. and Y. Y. Calculation: R. T. and C. S. Writing-original draft: Z. L. Writing-review & editing: Z. L., J. Z. and Y. Y.

Conflicts of interest

The authors declare no conflict of interest.

Data availability

The data that support the findings of this study are available from the corresponding author upon reasonable request.

Acknowledgements

The authors gratefully acknowledge the financial support from National Natural Science Foundation of China (No. 22379125, 22109030, and 22021001), Fundamental Research Funds for the Central Universities (20720220073), Fujian Industrial Technology Development and Application Plan (2022I0002), Key Research and Development Program Project of the Xinjiang Autonomous Region (2023B01025-1). The numerical calculations in this paper have been done on Hefei advanced computing center.

Notes and references

1. Y. Liu, X. Lu, F. Lai, T. Liu, P. R. Shearing, I. P. Parkin, G. He and D. J. L. Brett, *Joule*, 2021, **5**, 2845-2903.
2. C. Li, S. Jin, L. A. Archer and L. F. Nazar, *Joule*, 2022, **6**, 1733-1738.
3. S. Huang, R. Tang, X. Liu, Y. Zhang, Y. Tang, Z. Wen, M. Ye, Y. Yang and C. C. Li, *Energy Environ. Sci.*, 2024, **17**, 591-601.
4. C. S. of Electrochemistry, *Journal of Electrochemistry*, 2024, **30**, 2024121. DOI: 10.61558/2993-074X.3444.
5. M. Wu, C. Shi, J. Yang, Y. Zong, Y. Chen, Z. Ren, Y. Zhao, Z. Li, W. Zhang, L. Wang, X. Huang, W. Wen, X. Li, X. Ning, X. Ren and D. Zhu, *Adv. Mater.*, 2024, **36**, 2310434.
6. Y. Liu, C. Lu, Y. Yang, W. Chen, F. Ye, H. Dong, Y. Wu, R. Ma and L. Hu, *Adv. Mater.*, 2024, **36**, 2312982.
7. B. Tang, L. Shan, S. Liang and J. Zhou, *Energy Environ. Sci.*, 2019, **12**, 3288-3304.
8. Y. Kim, Y. Park, M. Kim, J. Lee, K. J. Kim and J. W. Choi, *Nat Commun*, 2022, **13**, 2371. View Article Online DOI: 10.1039/D4EE03857F
9. X. Zhang, Z. Deng, C. Xu, Y. Deng, Y. Jia, H. Luo, H. Wu, W. Cai and Y. Zhang, *Adv. Energy Mater.*, 2023, **13**, 2302749.
10. C. Meng, W.-D. He, H. Tan, X.-L. Wu, H. Liu and J.-J. Wang, *Energy Environ. Sci.*, 2023, **16**, 3587-3599.
11. Y. Dai, C. Zhang, J. Li, X. Gao, P. Hu, C. Ye, H. He, J. Zhu, W. Zhang, R. Chen, W. Zong, F. Guo, I. P. Parkin, D. J. L. Brett, P. R. Shearing, L. Mai and G. He, *Adv. Mater.*, 2024, **36**, 2310645.
12. W. Zhong, Z. Shen, J. Mao, S. Zhang, H. Cheng, Y. Kim and Y. Lu, *Energy Environ. Sci.*, 2024, **17**, 2059-2068.
13. X. Dou, X. Xie, S. Liang and G. Fang, *Sci. Bull.*, 2024, **69**, 833-845.
14. Z. Xing, G. Xu, J. Han, G. Chen, B. Lu, S. Liang and J. Zhou, *Trends Chem.*, 2023, **5**, 380-392.
15. S. Liu, R. Zhang, C. Wang, J. Mao, D. Chao, C. Zhang, S. Zhang and Z. Guo, *Angew. Chem. Int. Ed.*, 2024, **63**, e202400045.
16. K. Zhu, T. Wu and K. Huang, *Chem. Mater.*, 2021, **33**, 4089-4098.
17. D. S. Liu, Y. Zhang, S. Liu, L. Wei, S. You, D. Chen, M. Ye, Y. Yang, X. Rui, Y. Qin and C. C. Li, *Adv. Funct. Mater.*, 2022, **32**, 2111714.
18. Y. Wang, L. Yang, P. Xu, L. Liu, S. Li, Y. Zhao, R. Qin and F. Pan, *Small*, 2024, **20**, 2307446.
19. Q. Zhang, J. Luan, L. Fu, S. Wu, Y. Tang, X. Ji and H. Wang, *Angew. Chem. Int. Ed.*, 2019, **58**, 15841-15847.
20. H. Wang, W. Wei, X. Liu, S. Xu, Y. Dong and R. He, *Energy Storage Mater.*, 2023, **55**, 597-605.
21. H. Li, C. Han, Y. Huang, Y. Huang, M. Zhu, Z. Pei, Q. Xue, Z. Wang, Z. Liu, Z. Tang, Y. Wang, F. Kang, B. Li and C. Zhi, *Energy Environ. Sci.*, 2018, **11**, 941-951.
22. H. Li, Z. Liu, G. Liang, Y. Huang, Y. Huang, M. Zhu, Z. Pei, Q. Xue, Z. Tang, Y. Wang, B. Li and C. Zhi, *ACS Nano*, 2018, **12**, 3140-3148.
23. M. M. Ikhsan, S. Abbas, X. H. Do, H. Y. Ha, K. Azizi and D. Henkensmeier, *Adv. Energy Mater.*, 2024, 2400139. DOI: 10.1002/aenm.202400139.
24. M. Mara Ikhsan, S. Abbas, X. H. Do, S.-Y. Choi, K. Azizi, H. A. Hjuler, J. H. Jang, H. Y. Ha and D. Henkensmeier, *Chem. Eng. J.*, 2022, **435**, 134902.
25. Y. H. Wan, J. Sun, Q. P. Jian, X. Z. Fan and T. S. Zhao, *J. Mater. Chem. A*, 2022, **10**, 13021-13030.
26. X. H. Do, S. Abbas, M. M. Ikhsan, S. Y. Choi, H. Y. Ha, K. Azizi, H. A. Hjuler and D. Henkensmeier, *Small*, 2022, **18**, 2206284.
27. W. Lu, Z. Yuan, Y. Zhao, L. Qiao, H. Zhang and X. Li, *Energy Storage Mater.*, 2018, **10**, 40-47.
28. Z. Yuan, Y. Duan, H. Zhang, X. Li, H. Zhang and I. Vankelecom, *Energy Environ. Sci.*, 2016, **9**, 441-447.
29. J. Wu, C. Liao, T. Li, W. Lu, W. Xu, B. Ye, G. Li, H. Zhang and X. Li, *Adv. Energy Mater.*, 2023, **13**, 2300779.
30. L. Zou, K. Shi, H. Liu, Y. Wu, T. Xu, Q. Wang, Z. Chen, Z. Yang, R. Song, J. Su and W. Zhang, *Chem. Eng. J.*, 2023, **465**, 142794.
31. Y. Wang, T. Wang, D. Dong, J. Xie, Y. Guan, Y. Huang, J. Fan and Y.-C. Lu, *Matter*, 2022, **5**, 162-179.
32. H. Wang, A. Zhou, Z. Hu, X. Hu, F. Zhang, Z. Song, Y. Huang, Y. Cui, Y. Cui, L. Li, F. Wu and R. Chen, *Angew. Chem. Int. Ed.*, 2024, **63**, e202318928.

View Article Online
DOI: 10.1039/D4EE03857F

33. D. Jia, Z. Shen, Y. Lv, Z. Chen, H. Li, Y. Yu, J. Qiu and X. He, *Adv. Funct. Mater.*, 2024, **34**, 2308319.
34. Y. H. Lee, Y. Jeoun, J. H. Kim, J. Shim, K. S. Ahn, S. H. Yu and Y. E. Sung, *Adv. Funct. Mater.*, 2024, **34**, 2310884.
35. Y. Liu, Y. Sun, J. Zhang, X. Hao, M. Zhang, P. Wei, X. Zhao and K. Cai, *Nano Energy*, 2024, **120**, 109152.
36. R. Xue, Z. Wang, N. Yao, Y. Liu, H. Wang, M. Zhang, A. Shao, X. Tang, J. Liu, J. Tang, Z. Wang and Y. Ma, *Adv. Funct. Mater.*, 2024, **34**, 2400959.
37. C. Li, R. Kingsbury, A. S. Thind, A. Shyamsunder, T. T. Fister, R. F. Klie, K. A. Persson and L. F. Nazar, *Nat Commun*, 2023, **14**, 3067.
38. C. Wang, X. Zeng, J. Qu, J. M. Cairney, Q. Meng, P. J. Cullen and Z. Pei, *Matter*, 2023, **6**, 3993-4012.
39. Y. Wang, Z. Wang, W. K. Pang, W. Lie, J. A. Yuwono, G. Liang, S. Liu, A. M. D. Angelo, J. Deng, Y. Fan, K. Davey, B. Li and Z. Guo, *Nat Commun*, 2023, **14**, 2720.
40. X. Guo, J. Lu, M. Wang, A. Chen, H. Hong, Q. Li, J. Zhu, Y. Wang, S. Yang, Z. Huang, Y. Wang, Z. Pei and C. Zhi, *Chem*, 2024, **10**, 1-15. DOI: 10.1016/j.chempr.2024.07.028.
41. W. Wang, X. Zhang, S. Wu, B. Xu, S. Li, L. He, X. Li, Z. Chen, Y. Fan and A. L. R. Vellaisamy, *J. Raman Spectrosc.*, 2020, **51**, 2182-2191.
42. S. Deng, Y. Jiang, Y. Qu, A. Li, R. Zhang and Z. Xie, *Mater. Today Energy*, 2024, **44**, 101624.
43. D. Kundu, B. D. Adams, V. Duffort, S. H. Vajargah and L. F. Nazar, *Nat Energy*, 2016, **1**, 16119.
44. H. H. Kristoffersen and H. Metiu, *J. Phys. Chem. C*, 2016, **120**, 3986-3992.
45. Y. Wang, S. Wei, Z.-H. Qi, S. Chen, K. Zhu, H. Ding, Y. Cao, Q. Zhou, C. Wang, P. Zhang, X. Guo, X. Yang, X. Wu and L. Song, *Proc. Natl. Acad. Sci. U.S.A.*, 2023, **120**, e2217208120.
46. N. Zhang, Y. Dong, M. Jia, X. Bian, Y. Wang, M. Qiu, J. Xu, Y. Liu, L. Jiao and F. Cheng, *ACS Energy Lett.*, 2018, **3**, 1366-1372.
47. X. Wang, L. Ma, P. Zhang, H. Wang, S. Li, S. Ji, Z. Wen and J. Sun, *Appl. Surf. Sci.*, 2020, **502**, 144207.
48. S. Liu, J. Mao, W. K. Pang, J. Vongsvivut, X. Zeng, L. Thomsen, Y. Wang, J. Liu, D. Li and Z. Guo, *Adv. Funct. Mater.*, 2021, **31**, 2104281.

View Article Online
DOI: 10.1039/D4EE03857F

Data Availability Statement

The data that support the findings of this study are available from the corresponding author upon reasonable request.